npj | climate and atmospheric science

Article

Published in partnership with CECCR at King Abdulaziz University

https://doi.org/10.1038/s41612-024-00772-5

Multi-year La Niña frequency tied to southward tropical Pacific wind shift

Guojian Wang [1] & Agus Santoso [1,2,3]

Multi-year La Niña events cause prolonged climate disruptions worldwide, but a systematic understanding of the underlying mechanisms is not yet established. Here we show using observations and models from the sixth phase of Coupled Model Intercomparison Project that a greater frequency of consecutive La Niña events is tied to the upper equatorial Pacific Ocean when it favors more rapid heat discharge. The propensity for heat discharge is underscored by negative skewness in upper-ocean heat content, underpinned by southward tropical Pacific wind shift during austral summer. Models with stronger westerly anomalies south of the equator simulate steeper east-to-west upward tilt of the thermocline that is favorable for a greater discharge rate. This highlights the crucial role of the southward wind shift in the nonlinear system of the El Niño-Southern Oscillation. The large inter-model spread in multi-year La Niña processes underscores the need in constraining models for reliable climate prediction and projection.

As the earth's dominant year-to-year climate variability, El Niño-Southern Oscillation (ENSO) vacillates between El Niño and La Niña, with warmer and colder than normal sea surface temperature (SST) over the central-to-eastern equatorial Pacific Ocean, respectively[1]. The recharge-discharge oscillator is one of the classic ENSO theories to explain the oscillatory behavior of ENSO[2–4]. During El Niño events, the westerly wind anomalies over the western and central tropical Pacific Ocean induce eastward propagation of downwelling Kelvin waves, leading to eastward expansion of western Pacific warm pool, and a deepened thermocline in the eastern equatorial Pacific and a shoaled thermocline in the west. The anomalous westerlies subsequently promote a decrease of the upper equatorial Pacific Ocean heat content through poleward Sverdrup transport[2]. The discharge of the equatorial warm water terminates El Niño and favors a phase transition to a La Niña. In contrast, easterly wind anomalies during La Niña promote equatorward transport and recharges the tropical Pacific Ocean heat content, setting the stage for an El Niño.

ENSO exhibits asymmetric properties[5–9], not only in amplitude between El Niño and La Niña associated with a positive SST skewness in the eastern Pacific and a negative SST skewness in the central Pacific[8–14], but also in temporal evolution for which La Niña occurring for more than 1 year is more common than its El Niño counterpart[8,15–17]. Since the start of the 21st century, three multi-year La Niña sequences have occurred (Fig. 1A). Such long-lasting La Niña sequence has drawn much attention as it prolongs La Niña-associated global climate disruptions via teleconnection, e.g., frequent floods over eastern Australia and persistent drought in the United States[15,18–21]. Understanding the dynamics underpinning multi-year La Niña occurrences is of utmost importance for its near-term prediction and long-term projection.

Observational evidence has suggested that the La Niña associated recharge process tends to be weaker in amplitude compared to El Niño associated discharge[22–25], allowing for a longer duration of La Niña than El Niño[26–29]. Other studies offered various perspectives, including forcing from subsurface thermal anomalies[30–33], off-equator[34–39], inter-basin interaction[20,40], and meridional width of tropical Pacific SST pattern[41,42]. In general, there has been a lack of common understanding to explain multi-year La Niña occurrences, in particular with regards to observed decadal variations and inter-model diversity. This study discloses a strong link between the occurrences of multi-year La Niña and the tropical Pacific upper-ocean heat content in both observations and climate models.

Results

Observed multi-year La Niña

To revisit the historical La Niña years, we used the classic Niño3.4 SST index which covers SST anomalies over both the central-to-eastern tropical Pacific Ocean. We define an ENSO event as when Niño3.4 is greater than 0.75 standard deviation (s.d.) for both El Niño and La Niña (red and blue dots in Fig. 1A) during austral summer season (December, January, February, DJF). 21 La Niña events have occurred since 1948 in comparison with 14 El Niño. Around 70% (15 out of 21) La Niña belongs to seven multi-year La Niña sequences while no multi-year El Niño has been observed based on current

[1]CSIRO Environment, Aspendale, VIC, Australia. [2]Australian Research Council (ARC) Centre of Excellence for Climate Extremes and Climate Change Research Centre, Level 4 Mathews Building, The University of New South Wales, Sydney, NSW, Australia. [3]Frontiers Science Center for Deep Ocean Multispheres and Earth System (FDOMES), Ocean University of China, Qingdao, China. e-mail: guojian.wang@csiro.au; a.santoso@unsw.edu.au

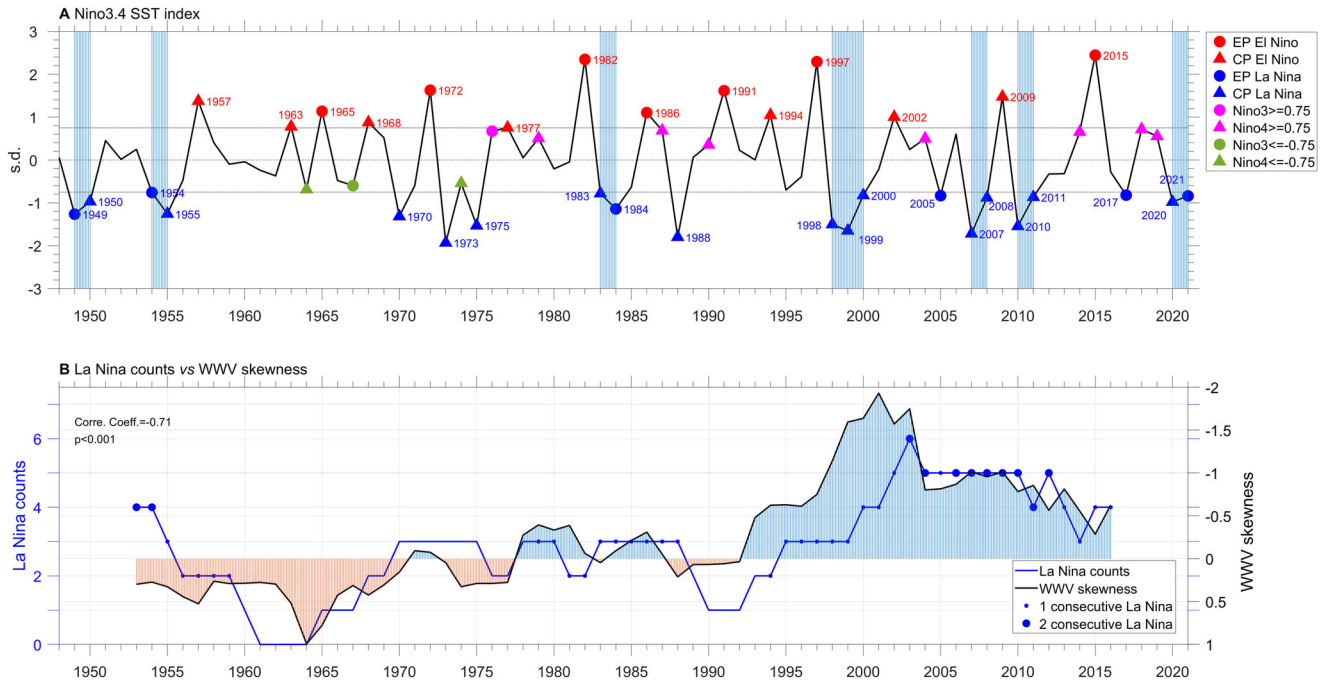

Fig. 1 | Observed decadal La Niña occurrences and decadal WWV skewness. **A** Niño3.4 SST index (170°W–120°W, 5°S–5°N) averaged over December, January, and February from HadISST[63]. El Niño (red dots) and La Niña (blue dots) events are defined as when Niño3.4 is greater than 0.75 standard deviation (s.d.). The consecutive La Nina sequence is indicated by the light blue vertical shades. Among those events, CP ENSO event is indicated by triangle when Niño4 (160°E–150°W, 5°S–5°N) is greater than Niño3 (150°W–90°W, 5°S–5°N) in amplitude and EP ENSO is indicated by circle when Niño4 is smaller than Niño3 (ref. 44). Beyond ENSO events captured by Niño3.4 index, additional CP and EP ENSO events are defined as when Niño4 and Niño3 index is greater than 0.75 s.d., respectively. **B** Time evolution of decadal La Niña occurrences and WWV skewness in 11-year sliding windows. The WWV is defined as the water volume with temperature above 20 °C over the domain of 120°E–80°W, 5°S–5°N[45]. The blue and orange shade indicates when WWV skewness is negative and positive, respectively. The blue dot indicates consecutive La Niña sequence over that 11-years window (center year) with the big size indicating two sequences and the small size indicating one sequence. The correlation coefficient between the two curves and the *p* value are also indicated. In observation, there is a tendency for multi-year La Niña event to occur more often when the tropical Pacific Ocean is easier to discharge than recharge.

criterion. In this study we define a multi-year event as when two or three La Niña happen in consecutive years. Among those consecutive sequences, two (1983–1984 and 1998–2000) were preceded by a strong El Niño in the year 1982 and 1997, defined as when Niño3.4 index is greater than 1.5 s.d., and five multi-year La Niña sequences (1949–1950, 1954–1955, 2007–2008, 2010–2011, and 2020–2022) did not follow a strong El Niño.

The identified relationship is not affected by different methods in defining an ENSO event, e.g., definition thresholds and ENSO regimes. Using different thresholds to define La Niña generates a similar relationship (Supplementary Fig. 1). The recent advance in understanding ENSO[43] has been based on categorizing ENSO into two different regimes with distinct dynamics, i.e., Central Pacific (CP) and Eastern Pacific (EP) ENSO, which could explain different impacts associated with the first and second La Niña in a multi-year event[18,19,21]. Utilizing Niño3 and Niño4 SST index, a CP ENSO event is defined as when Niño4 SST is greater than Niño3 SST (blue and red triangle in Fig. 1A), while an EP ENSO event is defined as when Niño3 SST is greater than Niño4 (blue and red circle in Fig. 1A) (ref. 44). There does not seem to be a clear preference in ENSO regime that precedes or follows one another in a multi-year event. Other events that could be captured by either Niño3 or Niño4 are also indicated (pink and green markers in Fig. 1A). Recounting La Niña events as when it passes the threshold for any Niño index does not influence the relationship between decadal WWV skewness and decadal La Niña frequency (Supplementary Fig. 2).

As limited by the length of observational record, here we count the La Niña occurrences using an 11-year sliding window which shows a decadal variation (blue curve in Fig. 1B). The choice of 11-year window is to include as many samples as possible in the analysis and the conclusion is not sensitive to 21-year and 31-year as alternatives. As ENSO is intimately linked to the background climate upon which it evolves[9], we propose that multi-year La Niña occurrences are tied to decadal variation in the tropical Pacific upper-ocean heat content. Here we use the conventional integrated warm water volume (WWV) above the 20 °C isotherm between 120°E–80°W, 5°S–5°N as a surrogate of the equatorial Pacific Ocean heat content[45,46], and calculate the WWV skewness for each of the 11-year window (black curve in Fig. 1B). There is a close relationship between the La Niña occurrences and WWV skewness across the decadal periods, with a correlation coefficient of −0.71 (note the reversed y-axis on the right-hand side): more La Niña occurrences tend to occur when the propensity leans towards a discharge state of the equatorial Pacific Ocean heat content. The contribution of consecutive La Niña sequences to the total La Niña occurrences is also highlighted, i.e., higher decadal La Niña occurrences coinciding with more consecutive La Niña sequences (blue dots in Fig. 1B). As such, the occurrences of multi-year La Niña events, although limited in numbers, appear to be related to the decadal WWV propensity. Replacing the WWV by ocean temperature integrated in the upper 300 m (T300) generates similar relationship (Supplementary Fig. 3). Below we show that climate models are able to generate an inter-model relationship between WWV skewness and multi-year La Niña frequency that is consistent with the observed relationship inferred from the relatively short observational record.

Simulated consecutive La Niña sequences

Using historical data from 33 coupled climate models that participated in the Coupled Model Intercomparison Project phase six (CMIP6) (ref. 47) (see "Methods" and Supplementary Table 1), we first count the multi-year La Niña occurrences over the entire 20th century due to the rareness of such multi-year La Niña events. Consistent with observed, there are two types of multi-year La Niña events that follow and do not follow a strong El Niño,

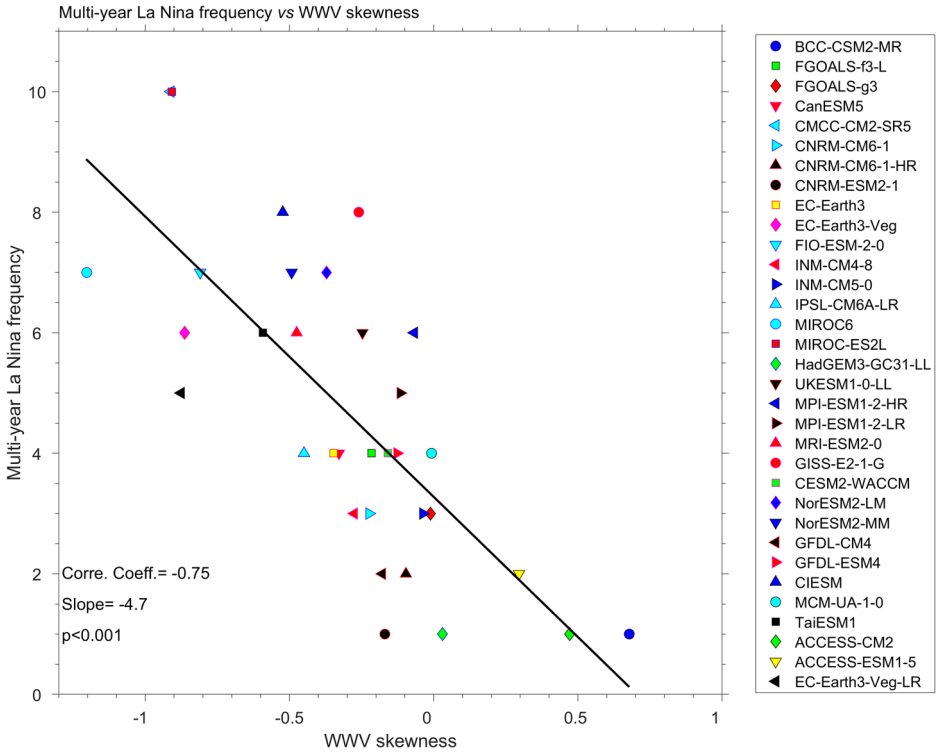

Fig. 2 | Simulated multi-year La Niña frequency and the WWV skewness over the 20th century. Inter-model relationship between the simulated multi-year La Niña frequency and the WWV skewness over 1900–1999. The correlation coefficient (Corre. Coeff.), slope, and *p* value are indicated. Consistent with observation, the strong inter-model relationship suggests that the greater propensity for the tropical Pacific Ocean to discharge, the more the multi-year La Niña tends to occur.

both contributing to the total occurrences of multi-year La Niña events (Supplementary Fig. 4A, B).

We also calculated WWV skewness which shows a close inter-model relationship with multi-year La Niña frequency (Fig. 2), indicating that models with greater negative WWV skewness tend to simulate more multi-year La Niña events. The inter-model correlation coefficients are all significant above 90% confidence level with various thresholds to define the La Niña (Supplementary Fig. 5). This underscores the preference of multi-year La Niña events for a discharge state in the upper tropical Pacific Ocean heat content, thus supporting the observed relationship. Below we show that the southward tropical Pacific wind shift during austral summer links WWV skewness and multi-year La Niña.

The observed and simulated southward wind shift

When an El Niño develops, the westerly wind anomalies over the tropical Pacific Ocean are symmetric about the equator. Through the air-sea feedback, the westerly anomalies eventually lead to El Niño peak in austral summer. As a response to the seasonal evolution in solar radiation, the zonal winds move southward to the south of the equator following the southward displacement of the tropical warm water[48,49]. As such, the symmetric pattern in zonal wind anomalies disappears during austral summer when El Niño matures[48–51]. The same happens for easterly wind anomalies during La Niña but with weaker magnitude than that during El Niño[52]. The southward wind shift contributes to the ENSO phase locking[7,48–54]. Here we found that the southward displaced zonal wind anomaly plays a key role in the simulated WWV skewness.

We first regressed zonal wind anomalies on Niño3.4 SST focusing on DJF season over the 20th century for each climate model. We then apply empirical orthogonal function (EOF) analysis[55] to the 33 fields of the ENSO-related zonal winds over the tropical Pacific Ocean (10°S–5°N, 130°E–80°W). The dominant EOF pattern reflects the southward wind shifts with anomalous westerlies south of the equator when El Niño matures (Fig. 3A). The corresponding principal component which represents the inter-model differences in the southward wind shift pattern is systematically linked to the WWV skewness; models simulating a greater westerly south of the equator tend to generate greater negative WWV skewness (Fig. 3B).

To elaborate on this point, we calculated the meridional heat transport using both subsurface temperature and oceanic meridional velocity for each model (see "Methods"). The net meridional heat transport is positive into and negative out of the tropical Pacific Ocean. We then regressed it against the inter-model differences in the southward wind shift pattern along the integrated boundary (north plus south). The inter-model regression pattern suggests that a model with greater westerly over the south of the equator simulates greater ocean heat discharge out of the tropical Pacific Ocean (Fig. 4A). The correlation coefficient between the inter-model difference in the southward wind shift and that in the recharge rate, calculated as the integration of the net meridional heat transport over the upper 300 m across the Pacific basin, is as high as −0.7 (Fig. 4B).

We further found that the inter-model relationship is through the modulation of the thermocline tilt along the tropical Pacific Ocean by the southward wind shift (Fig. 4C). A model simulating greater westerly during El Niño south of the equator is associated with the thermocline that is skewed shallow in the western tropical Pacific Ocean and skewed deep in the eastern tropical Pacific Ocean. Consistent with the thermocline-response-to-wind feedback[48,50,51], it implies that the southward wind shift could be the forcing for the propensity of the tropical Pacific Ocean heat content. Moreover, the positive relationship between heat discharge rate and multi-year La Niña frequency (greater heat discharge corresponding to higher frequency of multi-year La Niña events) strictly implies that the southward wind shift is the driver of multi-year La Niña, not the other way around (as multi-year La Niña would lead to a recharge state). As such, a greater westerly over the south of the equator is conducive for stronger heat discharge (more negative recharge rate), corresponding to greater negative WWV skewness (Fig. 3B) that is favorable to prolonged multi-year La Niña events (Fig. 2).

Such strong link between the southward wind shift and the WWV skewness is also captured by observation (Fig. 5). Applying sliding window of 11-yr long, we calculated the wind response during DJF. An EOF analysis was then applied to the multi-year zonal wind anomalies over the same domain as in models. The southward wind shift pattern in observation is similar to that simulated by models (Fig. 5A); when the westerly is greater south of the equator, there is a tendency for the WWV skewness to be more

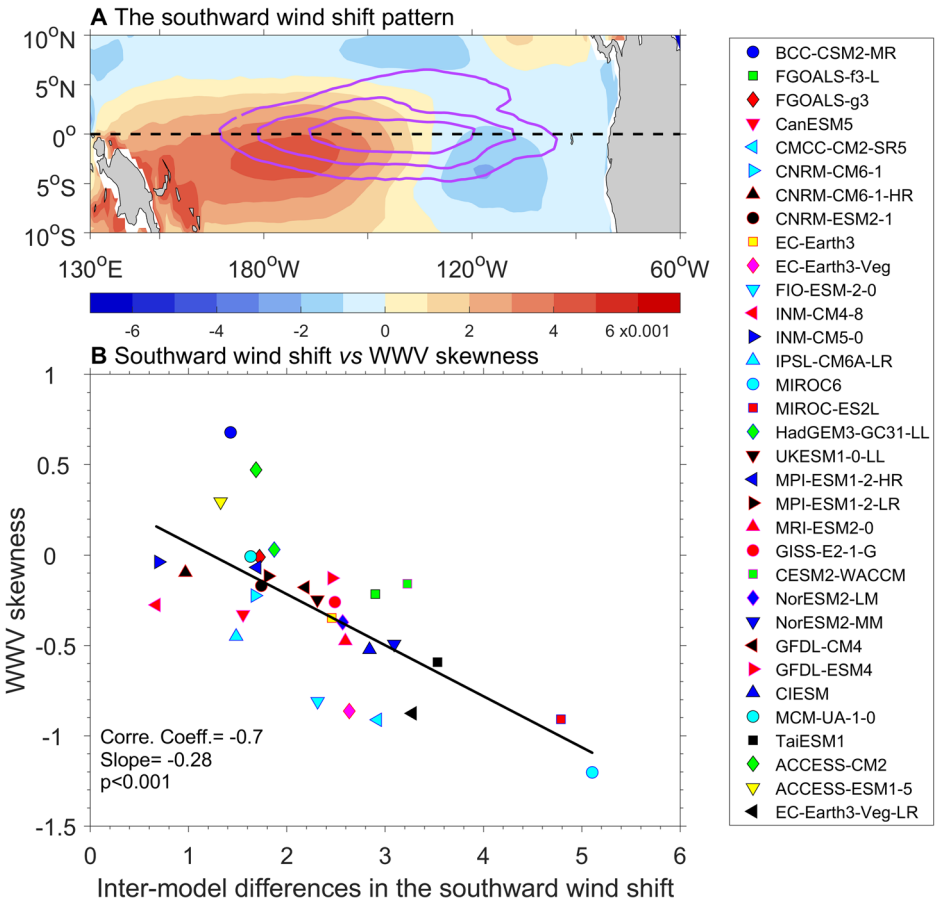

Fig. 3 | Inter-model differences in the southward wind shift pattern and its relationship with WWV skewness. An EOF analysis is applied to 33 patterns of 20th century ENSO-related zonal wind stress over the domain of (10°S–5°N, 130°E–80°W) from 33 CMIP6 models focusing on DJF season. **A** The first principal pattern (N m^{-2} s.d.$^{-1}$) describes inter-model differences in the southward wind shift pattern, explaining 34% of the total variance. The purple contours indicate positive SST anomalies associated with the principal component, highlighting symmetric SST anomalies about the equator in comparison to the southward wind shift. **B** An inter-model relationship of WWV skewness with the corresponding principal component (s.d.). The correlation coefficient, slope and *p* value are indicated. The inter-model differences in the southward wind shift can explain the inter-model spread in the WWV skewness.

negative (Fig. 5B). Using 31-yr and 51-yr sliding window produces similar results (Fig. 5C–F). This highlights the important role of the southward wind shift that is consistent between observation and models, as the mechanism governing the propensity of the tropical Pacific upper-ocean heat recharge and discharge.

Discussion

We explain the occurrences of multi-year La Niña events linked to the long-term mean state through processes internal to tropical Pacific Ocean[42], although the triggers can be external[20,36,38–41]. We found the observed multi-year La Niña frequency is tied to decadal WWV skewness (Fig. 1) in that greater negative WWV skewness is conducive to more prolonged La Niña events. Strong El Niño is conducive to prolonged La Niña in the following years by inducing stronger heat discharge, as such contributing to WWV skewness; there are also independent multi-year La Niña events that do not follow strong El Niño. The observed relationship is underpinned by a systematic inter-model relationship across 33 CMIP6 models between the multi-year La Niña frequency and WWV skewness (Fig. 2). A dynamical process further explains the relationship. First, we found that WWV skewness is governed by the southward tropical Pacific wind shift during ENSO mature season, with a greater westerly over the south of the equator setting up more favorable conditions for tropical Pacific Ocean heat discharge (Figs. 3 and 4). Therefore, the simulated multi-year La Niña frequency can be traced back to model's performance in the simulation of the southward wind shift. The key role of the southward wind shift in modulating changes in the ocean heat content is also evident in observation (Fig. 5). Our results reveal the southward wind shift during austral summer sets up the preference for oceanic heat recharge or discharge. This in turn affects the tendency for multi-year La Niña to occur, thus contributing to asymmetry in the frequency of multi-year El Niño and multi-year La Niña (Supplementary Fig. 6), highlighting the importance of the southward wind shift in ENSO asymmetry.

Consistent with previous studies suggesting that the southward tropical Pacific wind shift can influence the eastern equatorial Pacific thermocline depth[48,50,51], we further found that the systematic inter-model relationship is through the modulation of the thermocline tilt along the tropical Pacific Ocean by the southward wind shift (Fig. 4C). A greater ENSO nonlinearity (more negative; see "Methods") represents a more realistic ENSO simulation with more distinctive EP ENSO regime whose SST anomalies are skewed positive[56–61] (Supplementary Fig. 7). Models simulating greater westerly over the south of the equator are able to simulate more realistic ENSO nonlinearity (i.e., more negative, Fig. 4D), via the thermocline that is skewed deep in the eastern tropical Pacific Ocean through the thermocline-response-to-wind feedback.

We note that the inter-model spread in all of these processes and the multi-year La Niña frequency is large (Figs. 2, 3B, 4B–D). This study thus calls for more attention in the simulation of the southward tropical Pacific wind shift, as it is not only important to explain many ENSO-related phenomena, such as multi-year La Niña occurrences, but is also critical for realistic simulation of ENSO nonlinearity, thus for improved climate prediction and projection.

Methods

CMIP6 data and processing

To assess the possible relationship between multi-year La Niña frequency and WWV skewness, we take outputs from 33 CMIP6 models[47] (Supplementary Table 1) in which data are available in all fields including ocean temperatures, SST, and surface zonal wind stress. These models are forced under historical forcing emission scenarios. Before data analysis, the horizontal grids of each model are regridded to 1° × 1°; the oceanic vertical level is interpolated to upper 300 m with 10 m as interval. Monthly data from

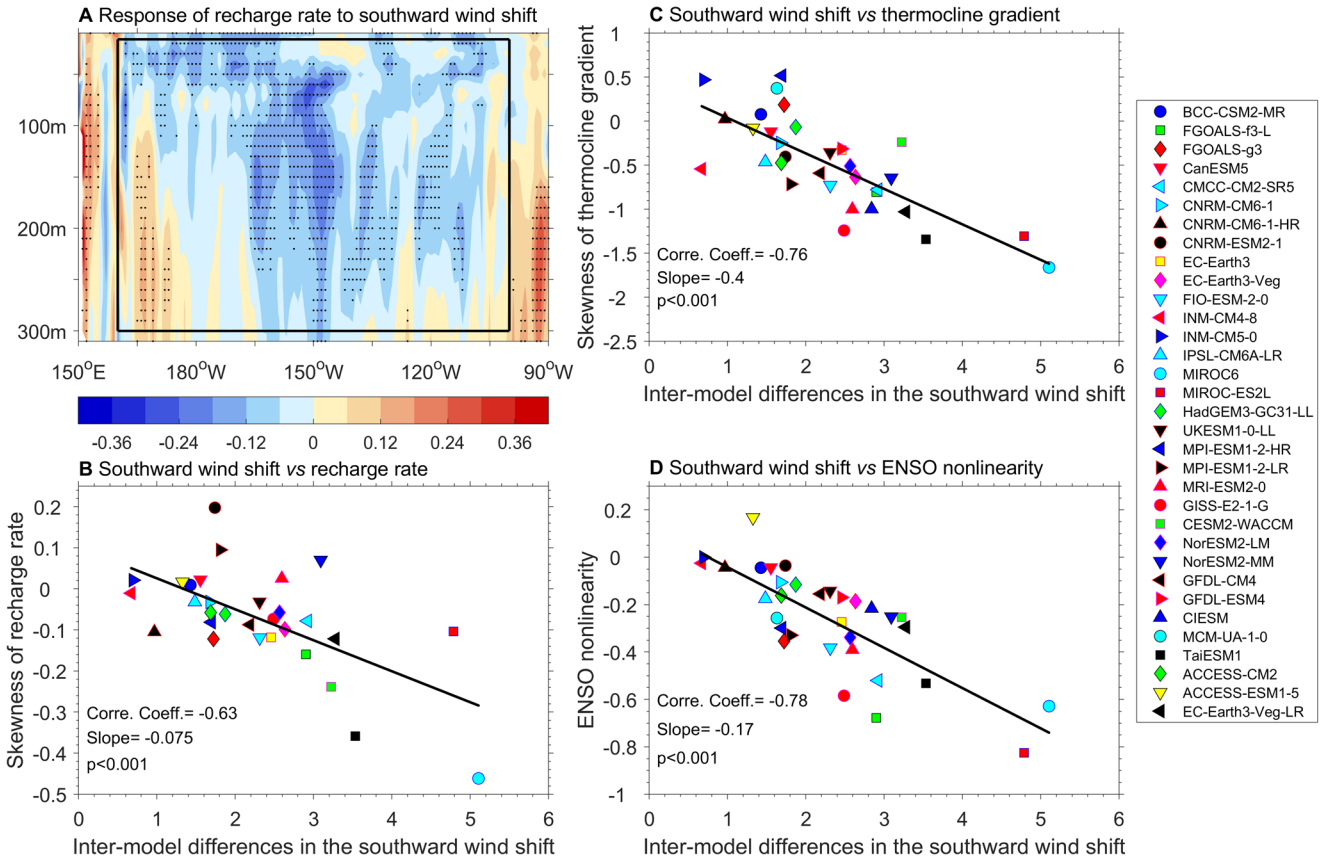

Fig. 4 | Inter-model relationship between southward wind shift pattern and tropical Pacific recharge rate. A Inter-model regression pattern of the skewness in net meridional heat transport along the integrated tropical Pacific boundary (see "Methods") onto inter-model differences in the southward wind shift pattern. The integrated vertical profile of the meridional heat transport is a summation of that along both 10°S and 10°N; as such it represents the net meridional heat transport into (positive) or out of (negative) the tropical Pacific Ocean. **B** Relationship between the inter-model differences in the southward wind shift pattern and the skewness of recharge rate integrated over the domain of (160°E–100°W, upper 300 m) as indicated by the black box in (**A**). The correlation coefficient, slope and *p* value are indicated. **C** The inter-model relationship between the southward wind shift and skewness of thermocline gradient. The thermocline gradient is calculated as the west-minus-east using thermocline depth averaged over the western tropical Pacific Ocean (5°S–5°N, 160°E–120°W) and the eastern tropical Pacific Ocean (5°S–5°N, 120°W–80°W). **D** The inter-model relationship between the southward wind shift and ENSO nonlinearity (α; see "Methods"). Models with greater negative α simulate stronger nonlinear Bjerknes feedback with more distinctive Central Pacific and Eastern Pacific ENSO regimes (see "Methods"). The inter-model differences in the southward wind shift governs the inter-model spread in the discharge-recharge propensity of the tropical Pacific Ocean heat content through its modulation on thermocline tilt across the tropical Pacific Ocean; it also contributes to ENSO nonlinearity, highlighting its important role in the nonlinear ENSO air-sea feedback.

1900 to 1999 are utilized. The oceanic meridional velocity is also utilized to calculate the recharge rate.

Observations

We use ocean temperature data from the Institute of Atmospheric Physics/Chinese Academy of Sciences[62] (IAP/CAS) to calculate the observed WWV skewness. SST and surface zonal wind stress are from Hadley Centre Sea Ice and Sea Surface Temperature dataset[63] (HadISST) and the National Centre for Environmental Prediction (NCEP)/National Centre for Atmospheric Research (NCAR) reanalysis 1 (ref. 64), respectively. Data covering 1948 onwards are used. Anomalies are referenced to the climatology over the full data period and then quadratically detrended for both model simulations and observations.

Meridional heat transport and recharge rate

To quantitatively evaluate the recharge and discharge of the tropical Pacific Ocean heat content, we calculated the net meridional heat transport[28] as follows:

$$T_v(depth, longitude) = -\rho CpT(depth, longitude) * vo(depth, lontitude)@10^{\circ}N + \rho CpT(depth, longitude) * vo(depth, lontitude)@10^{\circ}S$$

T_v is the net meridional heat transport across the tropical Pacific Ocean boundary (10°N and 10°S), indicating the ocean heat content into (positive) and out of (negative) of the tropical Pacific Ocean for any given time point. ρ is the reference density (1035 kg m^{-3}) and Cp is the specific heat capacity of seawater (3985 J kg^{-1} °C^{-1}). The first term on the right-hand side of the equation is the heat transport by the meridional velocity across 10°N (positive southward); the second term is the heat transport by the meridional velocity across 10°S (positive northward). Integration over the upper 300 m across the Pacific basin generates the recharge rate.

ENSO nonlinearity

For each model, we applied EOF analysis over the detrended tropical Pacific SST (15°S–15°N, 140°E–80°W). The first principal pattern exhibits a warm-anomaly center in the central-eastern Pacific and the second principal pattern shows a warm-anomaly center in the central Pacific and a cool-anomaly center in both the eastern and western parts of the basin[56]. The ENSO nonlinearity is determined by fitting the two corresponding principal components (PC) with the quadratic function:

$$PC2(t) = \alpha[PC1(t)]^2 + \beta PC1(t) + \gamma$$

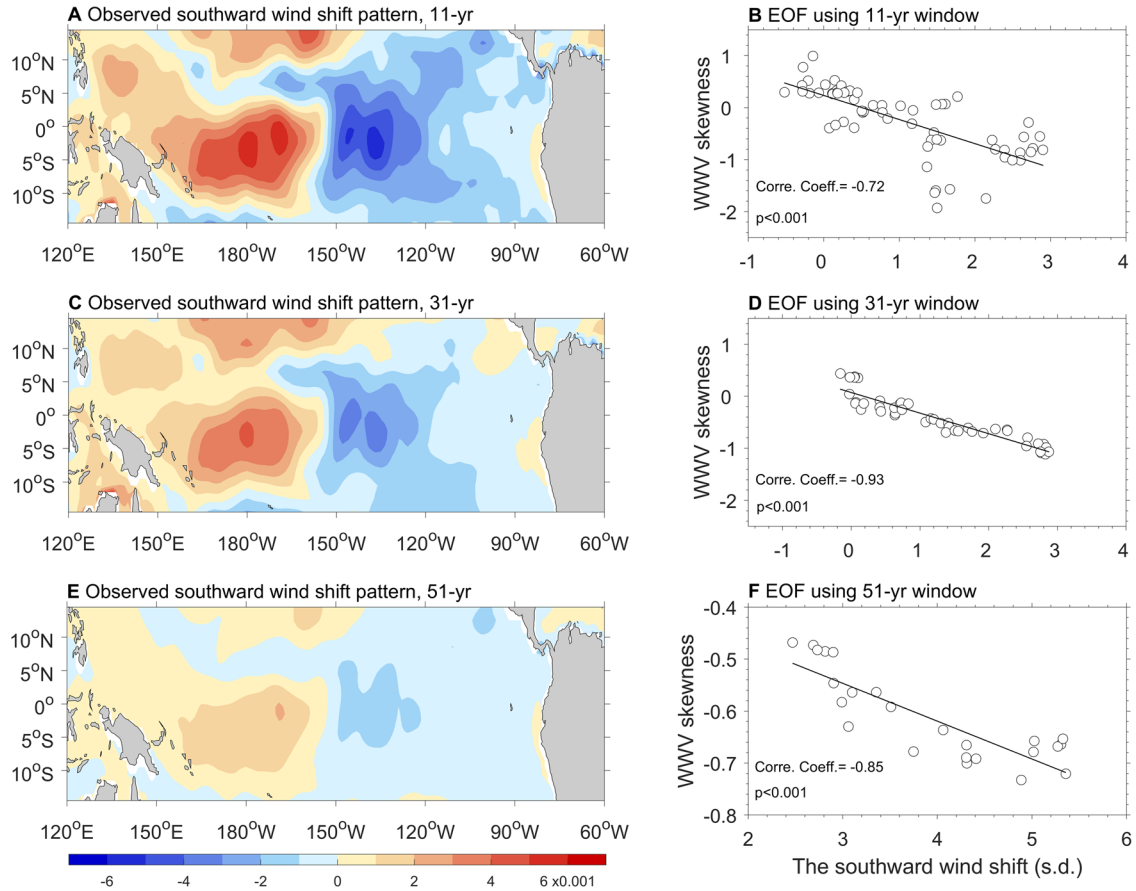

Fig. 5 | The impacts of decadal southward wind shift on decadal WWV skewness in observation. An empirical orthogonal function analysis is applied to the zonal wind response over the domain of (10°S–5°N, 130°E–80°W) based on an 11-yr, 31-yr, and 51-yr sliding window. **A** The first principal pattern represents the southward wind shift pattern using 11-yr sliding window. **B** The WWV skewness vs the corresponding principal component (s.d.). **C**, **D** and **E**, **F** The same as (**A**, **B**) but based on 31-yr and 51-yr sliding window, respectively. The impacts of southward wind shift on WWV skewness is also evident in observation.

Models with greater negative α systematically produce larger negative SST skewness in the Central Pacific and larger positive SST skewness in the Eastern Pacific, therefore, more realistic ENSO nonlinearity[56].

Statistical significance test

A bootstrap method[43] is used to evaluate the one-standard-deviation range in Supplementary Fig. 5. For each of La Niña threshold, 33 values from the 33 models are resampled randomly to construct 10,000 realizations of the correlation between multi-year La Niña frequency and WWV skewness. In this random resampling process, a model is allowed to be selected again. The standard deviation of the 10,000 inter-realizations of inter-model correlation coefficient is used for the uncertainty range.

Data availability

Data related to this paper can be downloaded from the following address. HadISST from https://www.metoffice.gov.uk/hadobs/hadisst/data/download.html; NCEP/NCAR Reanalysis 1 from https://psl.noaa.gov/data/gridded/data.ncep.reanalysis.html; IAP/CAS from http://159.226.119.60/cheng/; CMIP6 from https://pcmdi.llnl.gov/CMIP6/.

Code availability

All codes for the analysis are available upon request to the corresponding author in this paper.

Received: 7 March 2024; Accepted: 12 September 2024;
Published online: 30 September 2024

References

1. McPhaden, M. J., Zebiak, S. E. & Glantz, M. H. ENSO as an integrating concept in earth science. *Science* **314**, 1740–1745 (2006).
2. Jin, F.-F. An equatorial ocean recharge paradigm for ENSO. Part I: conceptual model. *J. Atmos. Sci.* **54**, 811–829 (1997).
3. Jin, F.-F. An equatorial ocean recharge paradigm for ENSO. Part II: a stripped-down coupled model. *J. Atmos. Sci.* **54**, 830–847 (1997).
4. Burgers, G. The simplest ENSO recharge oscillator. *Geophys. Res. Lett.* **32**, 22951 (2005).
5. Larkin, N. K. & Harrison, D. E. ENSO warm (El Niño) and cold (La Niña) event life cycles: ocean surface anomaly patterns, their symmetries, asymmetries, and implications. *J. Clim.* **15**, 1118–1140 (2002).
6. McPhaden, M. J. & Zhang, X. Asymmetry in zonal phase propagation of ENSO sea surface temperature anomalies. *Geophys. Res. Lett.* **36**, L13703 (2009).
7. McGregor, S. et al. Meridional movement of wind anomalies during ENSO events and their role in event termination. *Geophys. Res. Lett.* **40**, 749–754 (2013).
8. Choi, K.-Y., Vecchi, G. A. & Wittenberg, A. T. ENSO transition, duration, and amplitude asymmetries: role of the nonlinear wind stress coupling in a conceptual model. *J. Clim.* **26**, 9462–9476 (2013).
9. An, S.-I., Tziperman, E., Okumura, Y. M., Li, T. ENSO irregularity and asymmetry. In *El Niño Southern Oscillation in a Changing Climate* (eds McPhaden, M., Santoso, A., Cai, W.) Ch. 7, 153–172 (John Wiley & Sons, Inc, 2021).

10. Kang, I.-S. & Kug, J.-S. El Niño and La Niña sea surface temperature anomalies: asymmetry characteristics associated with their wind stress anomalies. *J. Geophys. Res.* **107**, 4372 (2002).
11. Wang, G. et al. Future Southern Ocean warming linked to projected ENSO variability. *Nat. Clim. Chang.* **12**, 649–654 (2022).
12. Chen, N., Fang, X. & Yu, J.-Y. A multiscale model for El Niño complexity. *npj Clim. Atmos. Sci.* **5**, 16 (2022).
13. Chen, N. & Fang, X. A simple multiscale intermediate coupled stochastic model for El Niño diversity and complexity. *J. Adv. Model. Earth Syst.* **15**, e2022MS003469 (2023).
14. Fang, X., Dijkstra, H., Wieners, C. & Guardamagna, F. A nonlinear full-field conceptual model for ENSO diversity. *J. Clim.* **37**, 3759–3774 (2024).
15. Cole, J. E., Overpeck, J. T. & Cook, E. R. Multiyear La Niña events and persistent drought in the contiguous United States. *Geophys. Res. Lett.* **29**, 1–4 (2002).
16. Okumura, Y. M., Ohba, M., Deser, C. & Ueda, H. A proposed mechanism for the asymmetric duration of El Niño and La Niña. *J. Clim.* **24**, 3822–3829 (2011).
17. Kim, J.-W. & Yu, J.-Y. Evolution of subtropical Pacific-onset El Niño: how its onset location controls its decay evolution. *J. Geophys. Res.* **48**, e2020GL091345 (2021).
18. Okumura, Y. M., DiNezio, P. & Deser, C. Evolving impacts of multiyear La Niña events on atmospheric circulation and U.S. drought. *Geophys. Res. Lett.* **44**, 11614–11623 (2017).
19. Iwakiri, T. & Watanabe, M. Multiyear La Niña impact on summer temperature over Japan. *J. Meteorol. Soc. Jpn. Ser. II* **98**, 1245–1260 (2020).
20. Hasan, N. A., Chikamoto, Y. & McPhaden, M. J. The influence of tropical basin interactions on the 2020-2022 double-dip La Nina. *Front. Clim.* **4**, 1001174 (2022).
21. Huang, G. et al. Seasonally evolving impacts of multiyear la niña on precipitation in Southern China. *Front. Earth Sci.* **10**, 884604 (2022).
22. Kessler, W. S. Is ENSO a cycle or a series of events? *Geophys. Res. Lett.* **29**, 2125 (2002).
23. Hu, Z.-Z. et al. Asymmetric evolution of El Niño and La Niña: the recharge/discharge processes and role of the off-equatorial sea surface height anomaly. *Clim. Dyn.* **49**, 2737–2748 (2017).
24. Li, X., Hu, Z.-Z., Zhao, S., Ding, R. & Zhang, B. The asymmetry of the tropical Pacific thermocline fluctuation associated with ENSO recharge and discharge. *Geophys. Res. Lett.* **49**, e2022GL099242 (2022).
25. Kim, J.-W., Yu, J.-Y. & Tian, B. Overemphasized role of preceding strong El Niño in generating multi-year La Niña events. *Nat. Commun.* **14**, 6790 (2023).
26. DiNezio, P. N. & Deser, C. Nonlinear controls on the persistence of La Niña. *J. Clim.* **27**, 7335–7355 (2014).
27. Wu, X., Okumura, Y. M. & DiNezio, P. N. What controls the duration of El Niño and La Niña events? *J. Clim.* **32**, 5941–5965 (2019).
28. Iwakiri, T. & Watanabe, M. Mechanisms linking multi-year La Niña with preceding strong El Niño. *Sci. Rep.* **11**, 17465 (2021).
29. Wang, B. et al. Understanding the recent increase in multiyear La Niñas. *Nat. Clim. Chang.* **13**, 1075–1081 (2023).
30. Zhang, R.-H., Rothstein, L. M. & Busalacchi, A. J. Origin of upper-ocean warming and El Niño change on decadal scales in the tropical Pacific Ocean. *Nature* **391**, 879–883 (1998).
31. Tang, Y. et al. Progress in ENSO prediction and predictability study. *Natl Sci. Rev.* **5**, 826–839 (2018).
32. Zhang, R.-H., Gao, C. & Feng, L. Recent ENSO evolution and its real-time prediction challenges. *Natl. Sci. Rev.* **9**, nwac052 (2022).
33. Gao, C., Chen, M., Zhou, L., Feng, L. & Zhang, R.-H. The 2020–2021 prolonged La Niña evolution in the tropical Pacific. *Sci. China Earth Sci.* **65**, 2248–2266 (2022).
34. Chiang, J. C. H. & Vimont, D. J. Analogous Pacific and Atlantic meridional modes of tropical atmosphere–ocean variability. *J. Clim.* **17**, 4143–4158 (2004).
35. Hu, Z.-Z., Kumar, A., Xue, Y. & Jha, B. Why were some La Niñas followed by another La Niña? *Clim. Dyn.* **42**, 1029–1042 (2014).
36. Zheng, F., Feng, L. & Zhu, J. An incursion of off-equatorial subsurface cold water and its role in triggering the "double dip" La Niña event of 2011. *Adv. Atmos. Sci.* **32**, 731–742 (2015).
37. Ding, R. et al. Multi-year El Niño events tied to the North Pacific Oscillation. *Nat. Commun.* **13**, 3871 (2022).
38. Geng, T. et al. Increased occurrences of consecutive La Niña events under global warming. *Nature* **619**, 774–781 (2023).
39. Fasullo, J. T. & Rosenbloom, N. A multiyear tropical Pacific cooling response to recent Australian wildfires in CESM2. *Sci. Adv.* **9**, eadg1213 (2023).
40. Luo, J.-J., Liu, G., Hendon, H., Alves, O. & Yamagata, T. Inter-basin sources for two-year predictability of the multi-year La Niña event in 2010–2012. *Sci. Rep.* **7**, 01479–01479 (2017).
41. Park, J.-H. et al. Mid-latitude leading double-dip La Niña. *Int. J. Climatol.* **41**, 1–18 (2020).
42. Iwakiri, T. & Watanabe, M. Multi-year ENSO dynamics as revealed in observations, climate model simulations, and the linear recharge oscillator. *J. Clim*. https://doi.org/10.1175/JCLI-D-22-0108.1 (2022).
43. Cai, W. et al. Changing El Niño–Southern Oscillation in a warming climate. *Nat. Rev. Earth Environ.* **2**, 628–644 (2021).
44. Yeh, S. W. et al. El Niño in a changing climate. *Nature* **461**, 511–514 (2009).
45. Meinen, C. S. & McPhaden, M. J. Observations of warm water volume changes in the equatorial Pacific and their relationship to El Niño and La Niña. *J. Clim.* **13**, 3551–3559 (2000).
46. McPhaden, M. J. Tropical Pacific Ocean heat content variations and ENSO persistence barriers. *Geophys. Res. Lett.* **30**, 1480 (2003).
47. Eyring, V. et al. Overview of the Coupled Model Intercomparison Project Phase 6 (CMIP6) experimental design and organization. *Geosci. Model Dev.* **9**, 1937–1958 (2016).
48. Lengaigne, M., Boulanger, J., Meinkes, C. & Spencer, H. Influence of the seasonal cycle on the termination of El Niño events in a coupled general circulation model. *J. Clim.* **19**, 1850–1868 (2006).
49. Vecchi, G. The termination of the 1997–98 El Niño. Part II: mechanisms of atmospheric change. *J. Clim.* **19**, 2647–2664 (2006).
50. Harrison, D. E. & Vecchi, G. A. On the termination of El Niño. *Geophys. Res. Lett.* **26**, 1593–1596 (1999).
51. Vecchi, G. & Harrison, D. E. On the termination of the 2002–03 El Niño event. *Geophys. Res. Lett.* **30**, 1964 (2003).
52. Stuecker, M. et al. A combination mode of the annual cycle and the El Niño/Southern Oscillation. *Nat. Geosci.* **6**, 540–544 (2013).
53. Abellan, E., McGregor, S. & England, M. H. Analysis of the southward wind shift of ENSO in CMIP5 models. *J. Clim.* **30**, 2415–2435 (2017).
54. McGregor, S., Timmermann, A., Schneider, N., Stuecker, M. F. & England, M. H. The effect of the South Pacific convergence zone on the termination of El Niño events and the meridional asymmetry of ENSO. *J. Clim.* **25**, 5566–5586 (2012).
55. Lorenz, E. N. *Empirical Orthogonal Functions and Statistical Weather Prediction* Statistical Forecast Project Report 1 (Massachusetts Institute of Technology, 1956).
56. Cai, W. et al. Increased variability of eastern Pacific El Niño under greenhouse warming. *Nature* **564**, 201–206 (2018).
57. Ham, Y.-G. El Niño events will intensify under global warming. *Nature* **564**, 192–193 (2018).
58. Takahashi, K., Montecinos, A., Goubanova, K. & Dewitte, B. ENSO regimes: reinterpreting the canonical and Modoki El Niño. *Geophys. Res. Lett.* **38**, L10704 (2011).

59. Dommenget, D., Bayr, T. & Frauen, C. Analysis of the non-linearity in the pattern and time evolution of El Niño Southern Oscillation. *Clim. Dyn.* **40**, 2825–2847 (2013).
60. Takahashi, K. & Dewitte, B. Strong and moderate nonlinear El Niño regimes. *Clim. Dyn.* **46**, 1627–1645 (2016).
61. Karamperidou, C., Jin, F.-F. & Conroy, J. L. The importance of ENSO nonlinearities in tropical Pacific response to external forcing. *Clim. Dyn.* **49**, 2695–2704 (2017).
62. Cheng, L. et al. Improved estimates of ocean heat content from 1960 to 2015. *Sci. Adv.* **3**, e1601545 (2017).
63. Rayner, N. A. et al. Global analyses of sea surface temperature, sea ice, and night marine air temperature since the late nineteenth century. *J. Geophys. Res. Atmos.* **108**, 4407 (2003).
64. Kalnay, E. et al. The NCEP/NCAR 40-year reanalysis project. *Bull. Am. Meteor. Soc.* **77**, 437–472 (1996).

Acknowledgements

We acknowledge the World Climate Research Programme's Working Group on Coupled Modeling, which led the design of CMIP6 and coordinated the work, and we also thank individual climate modeling group for their effort in model simulations and projections. G.W. and A.S. are supported by the Australian Government under the National Environmental Science Program.

Author contributions

G.W. and A.S. conceived the study and wrote the initial manuscript. G.W. performed data analysis and generated final figures.

Competing interests

The authors declare no competing interests.

Additional information

Supplementary information The online version contains supplementary material available at https://doi.org/10.1038/s41612-024-00772-5.

Correspondence and requests for materials should be addressed to Guojian Wang or Agus Santoso.